Accurate Extraction of Electrostatic Force by a Voltage-Pulse Force Spectroscopy

Eiichi Inami and Yoshiaki Sugimoto*
Graduate School of Engineering, Osaka University 2-1, Yamada-Oka, Suita, Osaka 565-0871, Japan
(Received 9 December 2014; revised manuscript received 13 February 2015; published 19 June 2015)

The classification of interaction forces between two approaching bodies is important in a wide range of research fields. Here, we propose a method to unambiguously extract the electrostatic force (F_{ele}), which is one of the most significant forces. This method is based on the measurement of the energy dissipation under applied voltage pulse between an atomic force microscopy (AFM) tip and sample. It allowed us to obtain F_{ele} as a function of the tip-sample distance and voltage including the distance-independent part, to which conventional AFM is insensitive. The obtained F_{ele} curves nicely fit the analytical model, enabling estimation of the geometry of the tip. The distance-dependent contact potential difference could also be correctly obtained by the measured F_{ele}, opening an alternative route to quantitative Kelvin probe force microscopy.

DOI: 10.1103/PhysRevLett.114.246102 PACS numbers: 68.37.Ps, 68.47.Fg

The interaction forces between two approaching objects is an important research subject in a wide range of fields. The various classes of forces include chemical bonding forces [1–4], Casimir forces [5,6], and non-Newtonian gravity forces [7]. Atomic force microscopy (AFM) is a highly sensitive tool that allows measurement of the interaction force (F) between its tip and a sample. Using a frequency modulation (FM) technique [8,9], F is usually estimated by measuring the frequency shift (Δf) as a function of the tip–surface distance (z) followed by mathematical conversion to $F(z)$.

One of the key issues in force measurement is the proper separation of the different physical origins of the measured F to extract desired forces as mentioned above. For instance, the separation between van der Waals force (F_{vdw}) and electrostatic force (F_{ele}) has been demonstrated [10,11], and is based on the measurement of Δf as a function of z as well as the bias voltage (V) between tip and sample. Extraction of F_{ele} itself is practically important in Kelvin probe force microscopy (KPFM), where the contact potential difference (V_{cpd}) between tip and sample is determined by the V minimizing F_{ele}. FM-KPFM is supposed to measure V_{cpd} from V to minimize $|\Delta f|$ [12,13]. However, the measurement of V_{cpd} as well as the extraction of F_{ele} are not trivial tasks [11] if V_{cpd} has a z dependence, as has frequently been observed in previous experiments [6,14–18]. The reason is as follows. F_{ele} is simply given by

$$F_{ele}(z, V) = a(z)[V - V_{cpd}(z)]^2 \quad (1)$$

using $a(z)$ as a function of z. This general form includes the V^2 term and V^1 term, which covers the charged system [19]. Hereafter, V is the sample bias with respect to the grounded tip. When V_{cpd} is independent of z, the z and V dependences on F_{ele} are separable. Then, the measured Δf has the same V dependence as F_{ele}; therefore, V_{cpd} can be estimated by the so-called Kelvin parabola of Δf. If V_{cpd} has a z dependence, this is not the case: the V dependence of Δf differs from that of F_{ele} [20]. In this case, the parabolic minimum in $\Delta f(V)$ does not coincide with V_{cpd}, as we prove later.

In this Letter, we propose a novel method to extract F_{ele} as a function of z and V reliably without measuring Δf. The method allows us to measure F_{ele} including a z-independent offset term, which is not observable in conventional AFM. By fitting into the analytical model, the tip radius and the cone angle can be estimated. It also enables us to correctly derive z-dependent V_{cpd}.

The principle for extracting $F_{ele}(z, V)$ is as follows. The force difference $[F_{\pm}(z)]$ between two different V values (here, $V = V_0 \pm V_p$ and $V = V_0$; $V_p > 0$) can be written by the difference in F_{ele} as below

$$F_{\pm}(z) = F_{ele}(z, V = V_0 \pm V_p) - F_{ele}(z, V = V_0) \quad (2)$$

since V-independent F, such as F_{vdw}, is canceled out. By substituting Eq. (1) into Eq. (2), we obtain

$$F_{\pm}(z) = a(z)V_p^2 \pm 2a(z)V_p[V_0 - V_{cpd}(z)]. \quad (3)$$

The function of $a(z)$ can be derived from the sum of $F_+(z)$ and $F_-(z)$ as

$$F_+(z) + F_-(z) = 2V_p^2 a(z). \quad (4)$$

From the obtained $a(z)$ and the difference between $F_+(z)$ and $F_-(z)$, $V_{cpd}(z)$ can be derived from the formula

$$F_+(z) - F_-(z) = 4V_p a(z)[V_0 - V_{cpd}(z)]. \quad (5)$$

Note that we can extract $F_{ele}(z, V)$, i.e. $a(z)$ and $V_{cpd}(z)$, by measuring $F_+(z)$ and $F_-(z)$ with any selection of V_0 or V_p.

One may try to obtain $F_\pm(z)$ by measuring $\Delta f(z)$ curves at three different V values ($V = V_0$, $V_0 + V_p$, and $V_0 - V_p$) followed by force conversion as in conventional force spectroscopy [21]. However, this method does not give an accurate $F_\pm(z)$ because a z-independent contribution is missing due to the insensitivity of Δf to constant force [11,34]. Note that Δf is sensitive to the force gradient, not to the force itself.

To extract F_{ele} including the offset, which is essential for correct estimation of V_{cpd} as explained later, we propose an alternative method. $F_\pm(z)$ is measured by the energy dissipation of the cantilever oscillation caused by voltage pulses to the surface. Figure 1(a) shows the schematics of our experimental setup. A cantilever is oscillated at constant amplitude (A) with resonance frequency (f). We applied square voltage pulses with an amplitude of V_p to the sample held at base voltage V_0. Pulse was applied at every cantilever oscillation cycle by using the cantilever deflection signal as a trigger. We defined the delay time of the pulse (τ) as the time from the tip's closest point to the surface. Under such a situation, the magnitude in F at $V = V_0$ jumps to that at $V = V_0 + V_p$ at the time of τ in only a short time period corresponding to the pulse width (w). Then, we could

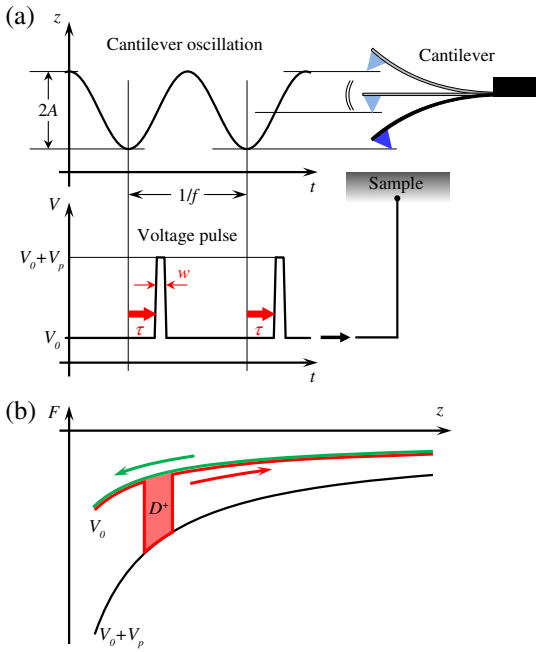

FIG. 1 (color online). (a) Schematic diagram of experimental setup of the voltage-pulse method for measurement of electrostatic force. Bias voltage pulse applied to the sample is synchronized with the cantilever oscillation. (b) Schematic $F(z)$ curves during cantilever oscillation. Forward and backward curves are shown by green and red, respectively. It is assumed that $|F(z, V = V_0 + V_p)|$ is larger than $|F(z, V = V_0)|$. Bias jump from V_0 to $V_0 + V_p$ produces hysteresis of F curves in each oscillation cycle. Energy dissipation D^+ is generated.

observe the energy dissipation corresponding to the area of the hysteresis loop as shown in Fig. 1(b), where $F(z)$ during tip approach and retraction are schematically shown by the green and red curves, respectively. Since w was set to be as small as a few tens of nanoseconds ($w \ll 1/f$), we could derive the linear relationship between the measured energy dissipation ($D_\pm$) and desired $F_\pm$ as below:

$$D_\pm(\tau) = -F_\pm[z = z(\tau)]w2\pi fA\sin(2\pi f\tau). \quad (6)$$

$D_\pm$ equals $F_\pm$ multiplied by the tip displacement during the pulse (product of cantilever speed and w). The validity of the linear relationship of Eq. (6) can be experimentally confirmed by the w dependence of $D_\pm(\tau)$ [21]. When $D_\pm(\tau)$ is measured under τ sweep from $-1/(2f)$ to $1/(2f)$, we can obtain $F_\pm(z)$ covering the z range of the cantilever oscillation. Thus, one can derive $a(z)$ and $V_{cpd}(z)$ in the z range of $2A$ from Eqs. (4) and (5).

To check the above idea, we performed experiments using our custom-built AFM operated at room temperature. Different kinds of samples, Si(111)-(7 × 7), Cu(001), and TiO_2(011), were used [21]. Commercial Pt-coated Si cantilevers were cleaned by Ar-ion sputtering in an ultrahigh vacuum (UHV). An optical interferometer was used for detection of cantilever deflection. The cantilever was oscillated at constant amplitude, typically $A = 10$ nm. We measured the oscillation spectrum for each cantilever used to check the cantilever dynamics. Our cantilever spectra were almost ideal [21]. Hence, we do not expect artificial dissipation due to an abnormal transfer function [35,36]. The voltage pulse was applied to the sample using a commercial function generator (Agilent 81180A). The energy dissipation was measured from the root mean square of the drive signal to maintain A in a cantilever oscillation controller [37]. The block diagram is shown elsewhere [21]. The high Q factor (typically 10 000) of the cantilevers in UHV enables us to detect the energy dissipation at a high signal-to-noise ratio [38]. We usually set V_0 to be close to the parabolic minimum of Δf. Since V_0 can be arbitrarily chosen as mentioned above, we do not have to know the V_{cpd} value *a priori*. The Si(111)-(7 × 7) surface was prepared by standard flashing and annealing. The Cu(001) and TiO_2(011) surfaces were prepared by sputtering and annealing cycles. The tip was located around the center of the terrace. During the τ sweep, the tip-surface distance feedback loop was opened. $D_+(\tau)$ and $D_-(\tau)$ were successively measured at the same z range using the same tip. The effect of changes of f (less than 0.1%) on $D_\pm(\tau)$ measurements during the τ sweep was negligibly small.

The $D_+(\tau)$ and $D_-(\tau)$ curves measured on the Si(111)-(7 × 7) surface are shown in Figs. 2(a) and 2(b), respectively. The delay time τ was swept over one cantilever oscillation cycle, i.e. $-1/(2f)$ to $1/(2f)$. At the turning points, i.e. $\tau = 0$, $-1/(2f)$, and $1/(2f)$, where the cantilever motion is stopped, $D_\pm$ becomes zero because of the lack of a hysteresis loop in the approach/retraction force

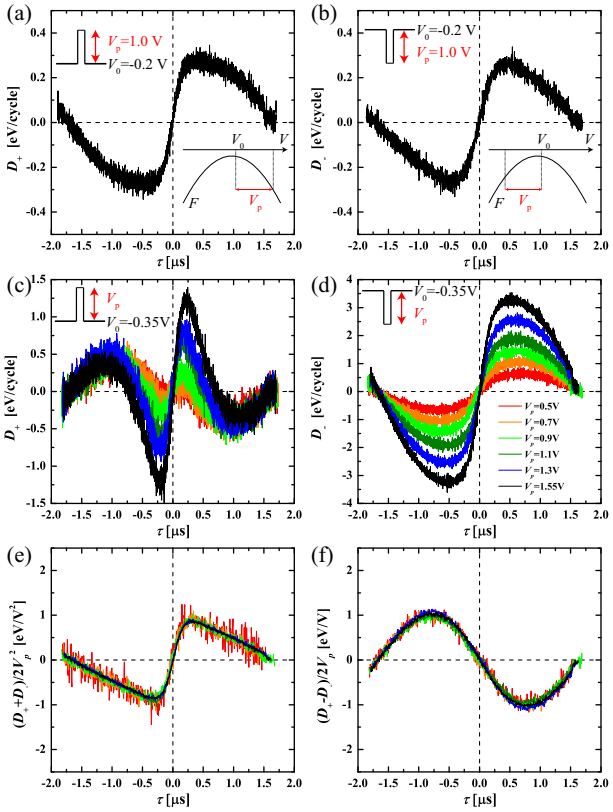

FIG. 2 (color online). (a) $D^+(\tau)$ and (b) $D^-(\tau)$ curves measured on the Si(111)-(7 × 7) surface. Pulse conditions and F vs V parabolic curves are schematically shown in the insets. (c) $D^+(\tau)$ and (d) $D^-(\tau)$ curves with different V_p values using a different cantilever from (a, b). (e) $(D^+ + D^-)/(2V_p^2)$ vs τ and (f) $(D^+ - D^-)/(2V_p)$ vs τ. We set $w = 50$ ns for all measurements. The acquisition parameters are summarized in the Supplemental Material [21].

curve. $D_\pm(\tau)$ is point symmetric for $\tau < 0$ and $\tau > 0$ since the energy gain and loss of the cantilever due to the pulse is simply inverted. For this particular example shown in Figs. 2(a) and 2(b), $D_+(\tau)$ looks similar to $D_-(\tau)$. This implies that a chosen V_0 (= −0.2 V) is close to the $V_{\rm cpd}$ (= −0.25 V almost independent of z as obtained later). Then, the responses to the pulses of $+V_p$ and $-V_p$ are symmetric as shown in the inset of Figs. 2(a) and 2(b).

Before calculating $F_{\rm ele}(z)$ from $D_\pm(\tau)$, we verify the method and the equations above. Figures 2(c) and 2(d) show $D_+(\tau)$ and $D_-(\tau)$ curves, respectively, which were measured by various V_p values (from 0.5 to 1.55 V) keeping $V_0 = -0.35$ V. We used a different cantilever from that used in Figs. 2(a) and 2(b). While $D_\pm = 0$ at the turning points and the point symmetry around $\tau = 0$ are seen as discussed above, the shape of $D_+(\tau)$ in Fig. 2(c) looks different from the simple form shown in Fig. 2(a). D_+ changes sign even within either $\tau < 0$ or $\tau > 0$. This is due to the intersection of the $F_{\rm ele}(z, V = V_0 + V_p)$ curve and the $F_{\rm ele}(z, V = V_0)$ curve. This intersection implies that $V_{\rm cpd}$ depends on z as clarified later. Figures 2(e) and 2(f) show $(D_+ + D_-)/2V_p^2$ and $(D_+ - D_-)/2V_p$ curves, respectively, which were calculated from the curves in Figs. 2(c) and 2(d). Remarkably, all curves obtained by different V_p values collapse into a single curve in both Figs. 2(e) and 2(f). These scalings by V_p^2 and V_p confirm the validity of the measurement principle shown in Eqs. (4)–(6). This result also eliminates other dissipation mechanisms such as Joule heating dissipation [39] and apparent dissipation caused by phase error [35,36].

Since $D_\pm$ is related to $F_\pm$ by Eq. (6), the curves in Fig. 2(e) and 2(f) can be converted into $(F_+ + F_-)/2V_p^2$ and $(F_+ - F_-)/2V_p$, respectively. Then, we can obtain $a(z)$ and $V_{\rm cpd}(z)$ using Eqs. (4)–(5). Figures 3(a) and 3(b) display the data obtained by eight different tips including tip 1 and tip 2 used for Figs. 2(a) and 2(b) and Figs. 2(c–f), respectively. It is worth mentioning that both $a(z)$ and $V_{\rm cpd}(z)$ curves are obtained by the τ sweep instead of the z sweep as in conventional force spectroscopy. The distance z is covered in the range of the cantilever swing (i.e., $2A$).

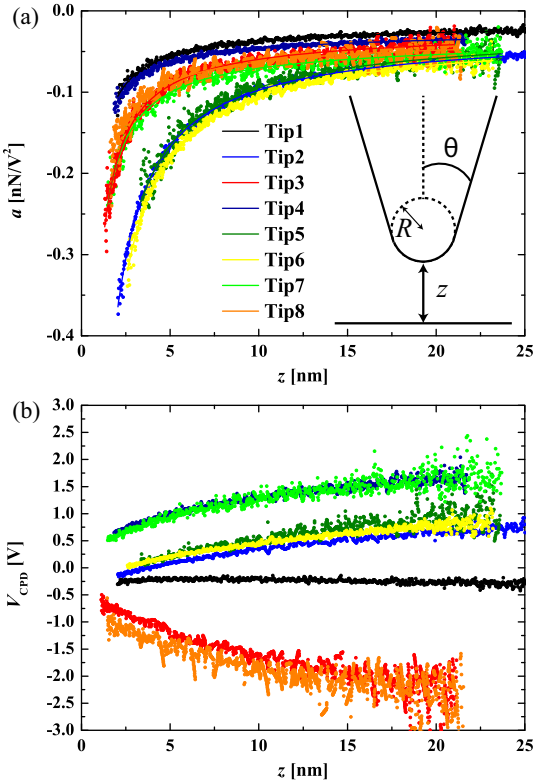

FIG. 3 (color online). (a) Extracted $a(z)$ and (b) $V_{\rm cpd}(z)$ curves with eight different tips. Tip 1 and tip 2 correspond to Figs. 2(a) and 2(b) and Figs. 2(c–f), respectively. The fitting curves based on Eq. (7) are shown in (a). The values of R (θ) are determined to be 6.0 nm (6.2°), 24.7 nm (12.9°), 11.1 nm (11.3°), 5.7 nm (11.2°), 25.2 nm (10.5°), 27.0 nm (13.6°), 10.2 nm (16.7°), and 8.5 nm (15.3°) for tips 1–8, respectively. The tip model is illustrated in the inset. $z = 0$ is defined as the divergence point of $a(z)$. The acquisition parameters are summarized in the Supplemental Material [21].

In contrast to conventional force spectroscopy based on a $\Delta f(z)$ measurement, the present technique can provide $F_{\rm ele}(z)$ including the offset term, i.e., the z-independent contribution [see Fig. 3(a)]. All $a(z)$ curves asymptotically approach nonzero constant values at large z values. This offset has not been measured in previous experiments [10,11]. We found that all of the $a(z)$ curves we obtained could be fitted well into the analytical model [40] based on a plane and a truncated cone ending in a spherical cap as illustrated in the inset in Fig. 3(a). Assuming that a sample is equipotential, it can be written as

$$a(z) = -\pi\epsilon_0\left\{\frac{R^2(1-\sin\theta)}{z[z+R(1-\sin\theta)]} + \beta^2\left[-\ln\frac{z+R(1-\sin\theta)}{L} - 1 + \frac{R\cos^2\theta/\sin\theta}{z+R(1-\sin\theta)}\right]\right\}, \quad (7)$$

where $\beta^2 = [\ln\tan(\theta/2)]^{-2}$. ϵ_0, R, θ, and L are the dielectric constant in the vacuum, tip radius, cone opening angle, and tip length, respectively. The first term in Eq. (7) represents the contribution from the truncated sphere of the tip apex, which has z^{-1} dependence in the close-distance regime ($z \ll R$). The other terms show the contribution of the cone part, which produces the offset force. The fitting curves are shown in Fig. 3(a). L is fixed as 17 μm taken from the data sheet of the cantilever. R and θ can be precisely determined as fitting parameters (see the caption of Fig. 3). The obtained values in R and θ are in good agreement with the data sheet of the cantilever, i.e. $R < 25$ nm and $\theta \approx 10°$. Therefore, one can estimate the tip shape by the present method.

Next, we discuss the $V_{\rm cpd}(z)$ curves that we obtained. $V_{\rm cpd}(z)$ with tip 1 corresponding to Figs. 2(a) and 2(b) is almost z independent [see the black plots in Fig. 3(b)] while the other $V_{\rm cpd}(z)$ curves have clear z dependence. $V_{\rm cpd}$ decreases with decreasing z for tips 2 and 4–7 while $V_{\rm cpd}$ increases for tips 3 and 8. In all curves, as the distance decreased, $V_{\rm cpd}$ approached the value of z-independent $V_{\rm cpd}$ obtained by tip 1. This can be explained by the averaging effect, as observed in previous studies [14–17]. In the present experiments, the averaging effect originates in the tip, since the Si(111)-(7 × 7) surface is homogeneous. At far tip-surface distances, all parts of the tip including the tip sides contribute to $V_{\rm cpd}$. At closer tip-surface distances, the tip apex plays a main role in $V_{\rm cpd}$ while the tip sides exert less effect. Therefore, the $V_{\rm cpd}$ values obtained by the different tips are similar to each other at small z. Empirically, tip-surface contacts (intentional or accidental) tend to produce such z dependence in $V_{\rm cpd}$. Inhomogeneous work function on the tip may be caused by multiple facets, trapped charges, and patch charges [41].

Finally, we experimentally compare the pulse method and conventional FM-KPFM to see the difference between $V_{\rm cpd}$ and signal in FM-KPFM ($V_{\rm cpd}^{FM}$). $\Delta f(V)$ curves were measured at different z on the Cu(001) surface [see Fig. 4(a)]. $V_{\rm cpd}^{FM}(z)$ extracted from V to minimize $|\Delta f(V)|$ was plotted in Fig. 4(b) (blue plots). Then, we carried out pulse experiments on the same surface site with the same tip state. After the same analysis as described above, we obtained $V_{\rm cpd}(z)$ as shown in Fig. 4(b) (black curve). It is clearly shown that $V_{\rm cpd}^{FM}(z)$ is deviated from $V_{\rm cpd}(z)$. Since $F_{\rm ele}(z, V)$ obtained by the pulse method can be numerically converted into $\Delta f(z, V)$, $V_{\rm cpd}^{FM}$ can be also simulated from results of pulse experiments. We used the same oscillation parameters for the simulation as the FM-KPFM experiment. The simulated $V_{\rm cpd}^{FM}(z)$ is shown in Fig. 4(b) (dashed green curve). The simulated curve matches the experimental plots quite well. It was demonstrated that $V_{\rm cpd}^{FM}(z)$ is different from $V_{\rm cpd}(z)$ if $V_{\rm cpd}(z)$ has a z dependence. Further details are discussed in the Supplemental Material [21].

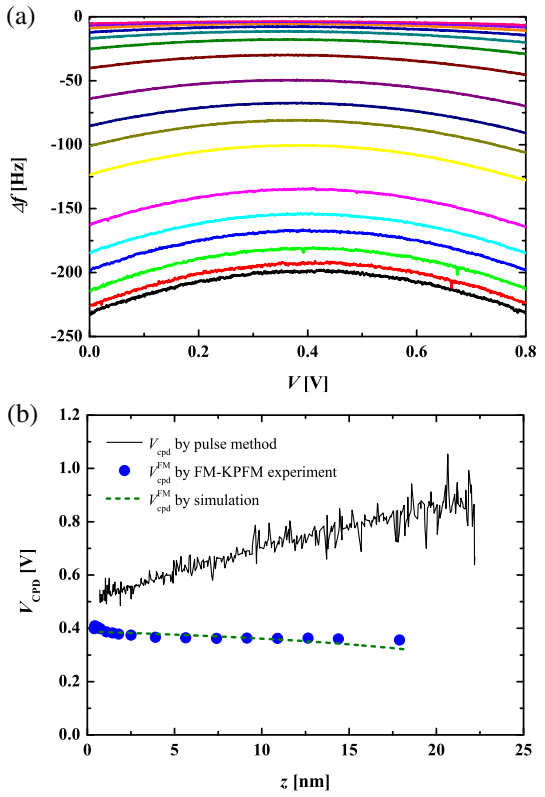

FIG. 4 (color online). (a) FM-KPFM measurements: $\Delta f(V)$ curves at different heights on the Cu(001) surface. (b) $V_{\rm cpd}(z)$ obtained by pulse method (black curve) and $V_{\rm cpd}^{FM}(z)$ obtained by FM-KPFM experiments of (a) (blue circles). The simulated $V_{\rm cpd}^{FM}(z)$ is also shown by the green curve. One cannot calculate $V_{\rm cpd}^{FM}(z)$ at far distances in the region of $2A$ since $F_{\rm ele}$ data are missing to calculate Δf in this region. The acquisition parameters for pulse measurements were $f = 287480.6$ Hz, $A = 125$ Å, and $k = 26.3$ N/m, respectively. A is reduced to $A = 19.6$ Å for FM-KPFM measurements, and for the simulation of $V_{\rm cpd}^{FM}(z)$.

We have developed a voltage-pulse AFM technique to obtain F_{ele} as a function of z and V. This method based on dissipation measurement enables us to determine F_{ele} with the offset, which can be directly fitted into the analytical model to estimate the tip geometry. Furthermore, z-dependent V_{cpd} can be accurately measured. Using the proposed technique, it is expected that charge states, local work functions, and field-induced effects on surfaces can be quantitatively investigated. Correct estimation of F_{ele} is also essential to extract desired forces such as Casimir forces and the gravity forces.

We wish to thank S. Kawai, K. Kobayashi, L. Gross, and S. Sadewasser for fruitful discussions. This work was supported by Grants-in-Aid for Scientific Research (No. 15H03566, No. 26600015, No. 26110516) from the Ministry of Education, Culture, Sports, Science and Technology of Japan (MEXT), Funding Program for Next Generation World-Leading Researchers.

*ysugimoto@k.u-tokyo.ac.jp

[1] M. A. Lantz, H. J. Hug, R. Hoffmann, P. J. A. van Schendel, P. Kappenberger, S. Martin, A. Baratoff, and H. J. Guntherodt, Science **291**, 2580 (2001).
[2] Y. Sugimoto, P. Pou, M. Abe, P. Jelinek, R. Perez, S. Morita, and O. Custance, Nature (London) **446**, 64 (2007).
[3] M. Ternes, C. Gonzalez, C. P. Lutz, P. Hapala, F. J. Giessibl, P. Jelinek, and A. J. Heinrich, Phys. Rev. Lett. **106**, 016802 (2011).
[4] Y. Sugimoto, M. Ondracek, M. Abe, P. Pou, S. Morita, R. Perez, F. Flores, and P. Jelinek, Phys. Rev. Lett. **111**, 106803 (2013).
[5] S. K. Lamoreaux, Phys. Rev. Lett. **78**, 5 (1997).
[6] W. J. Kim, A. O. Sushkov, D. A. R. Dalvit, and S. K. Lamoreaux, Phys. Rev. Lett. **103**, 060401 (2009).
[7] E. G. Adelberger, B. R. Heckel, and A. E. Nelson, Annu. Rev. Nucl. Part. Sci. **53**, 77 (2003).
[8] T. R. Albrecht, P. Grütter, D. Horne, and D. Rugar, J. Appl. Phys. **69**, 668 (1991).
[9] *Noncontact Atomic Force Microscopy*, edited by S. Morita, F. J. Giessibl, and R. Wiesendanger (Springer-Verlag, Berlin, 2009), Vol. 2.
[10] M. Guggisberg, M. Bammerlin, C. Loppacher, O. Pfeiffer, A. Abdurixit, V. Barwich, R. Bennewitz, A. Baratoff, E. Meyer, and H.-J. Guntherodt, Phys. Rev. B **61**, 11151 (2000).
[11] J. Falter, G. Langewisch, H. Holscher, H. Fuchs, and A. Schirmeisen, Phys. Rev. B **87**, 115412 (2013).
[12] S. Kitamura and M. Iwatsuki, Appl. Phys. Lett. **72**, 3154 (1998).
[13] *Kelvin Probe Force Microscopy*, edited by S. Sadewasser and T. Glatzel (Springer, Heidelberg, Dordrecht, London, New York, 2011).
[14] C. Sommerhalter, T. Glatzel, T. W. Matthes, A. Jager-Waldau, and M. C. Lux-Steiner, Appl. Surf. Sci. **157**, 263 (2000).
[15] U. Zerweck, C. Loppacher, T. Otto, S. Grafstrom, and L. M. Eng, Phys. Rev. B **71**, 125424 (2005).
[16] T. Konig, G. H. Simon, H. P. Rust, and M. Heyde, J. Phys. Chem. C **113**, 11301 (2009).
[17] R. Baier, C. Leendertz, M. Ch. Lux-Steiner, and S. Sadewasser, Phys. Rev. B **85**, 165436 (2012).
[18] A. Yurtsever, Y. Sugimoto, M. Fukumoto, M. Abe, and S. Morita, Appl. Phys. Lett. **101**, 083119 (2012).
[19] R. Stomp, Y. Miyahara, S. Schaer, Q. Sun, H. Guo, P. Grutter, S. Studenikin, P. Poole, and A. Sachrajda, Phys. Rev. Lett. **94**, 056802 (2005).
[20] L. Nony, A. S. Foster, F. Bocquet, and C. Loppacher, Phys. Rev. Lett. **103**, 036802 (2009).
[21] See Supplemental Material at http://link.aps.org/supplemental/10.1103/PhysRevLett.114.246102, which includes Refs. [22–33].
[22] L. Gross, F. Mohn, P. Liljeroth, J. Repp, F. J. Giessibl, and G. Meyer, Science **324**, 1428 (2009).
[23] F. Bocquet, L. Nony, and C. Loppacher, Phys. Rev. B **83**, 035411 (2011).
[24] F. Mohn, L. Gross, N. Moll, and G. Meyer, Nat. Nanotechnol. **7**, 227 (2012).
[25] A. Sasahara, C. Pang, and H. Onishi, J. Phys. Chem. B **110**, 17584 (2006).
[26] H. J. Chung, A. Yurtsever, Y. Sugimoto, M. Abe, and S. Morita, Appl. Phys. Lett. **99**, 123102 (2011).
[27] J. Onoda, C. Pang, A. Yurtsever, and Y. Sugimoto, J. Phys. Chem. C **118**, 13674 (2014).
[28] S. Sadewasser, P. Jelinek, C. K. Fang, O. Custance, Y. Yamada, Y. Sugimoto, M. Abe, and S. Morita, Phys. Rev. Lett. **103**, 266103 (2009).
[29] A. Kikukawa, S. Hosaka, and R. Imura, Appl. Phys. Lett. **66**, 3510 (1995).
[30] T. Glatzel, S. Sadewasser, and M. Lux-Steiner, Appl. Surf. Sci. **210**, 84 (2003).
[31] S. Kawai, T. Glatzel, H.-J. Hug, and E. Meyer, Nanotechnology **21**, 245704 (2010).
[32] Y. Sugimoto, I. Yi, K. Morita, M. Abe, and S. Morita, Appl. Phys. Lett. **96**, 263114 (2010).
[33] J. E. Sader and S. P. Jarvis, Appl. Phys. Lett. **84**, 1801 (2004).
[34] F. J. Giessibl, Phys. Rev. B **56**, 16010 (1997).
[35] A. Labuda, Y. Miyahara, L. Cockins, and P. H. Grutter, Phys. Rev. B **84**, 125433 (2011).
[36] S. Kawai, T. Glatzel, B. Such, S. Koch, A. Baratoff, and E. Meyer, Phys. Rev. B **86**, 245419 (2012).
[37] N. Oyabu, P. Pou, Y. Sugimoto, P. Jelinek, M. Abe, S. Morita, R. Pérez, and O. Custance, Phys. Rev. Lett. **96**, 106101 (2006).
[38] T. Fukuma, K. Kobayashi, H. Yamada, and K. Matsushige, Rev. Sci. Instrum. **75**, 4589 (2004).
[39] W. Denk and D. W. Pohl, Appl. Phys. Lett. **59**, 2171 (1991).
[40] S. Hudlet, M. S. Jean, C. Guthmann, and J. Berger, Eur. Phys. J. B **2**, 5 (1998).
[41] N. A. Burnham, R. J. Colton, and H. M. Pollock, Phys. Rev. Lett. **69**, 144 (1992).